



# Assessment of malignant potential in intraductal papillary mucinous neoplasms of the pancreas using MR findings and texture analysis

Sun Kyung Jeon<sup>1</sup> · Jung Hoon Kim<sup>1,2,3</sup> · Jeongin Yoo<sup>1</sup> · Ji-Eun Kim<sup>1</sup> · Sang Joon Park<sup>1</sup> · Joon Koo Han<sup>1,2,3</sup>

Received: 4 June 2020 / Revised: 25 August 2020 / Accepted: 14 October 2020 / Published online: 2 November 2020

© European Society of Radiology 2020

## Abstract

**Objectives** To investigate the utility of MR findings and texture analysis for predicting the malignant potential of pancreatic intraductal papillary mucinous neoplasms (IPMNs).

**Methods** Two hundred forty-eight patients with surgically confirmed IPMNs (106 malignant [invasive carcinoma/high-grade dysplasia] and 142 benign [low/intermediate-grade dysplasia]) and who underwent magnetic resonance imaging (MRI) with MR cholangiopancreatography (MRCP) were included. Two reviewers independently analyzed MR findings as proposed by the 2017 international consensus guidelines. Texture analysis of MRCP was also performed. A multivariate logistic regression analysis was used to identify predictors for malignant IPMNs. Diagnostic performance was also analyzed using receiver operating curve analysis.

**Results** Among MR findings, enhancing mural nodule size  $\geq 5$  mm, main pancreatic duct (MPD)  $\geq 10$  mm or MPD of 5 to 9 mm, and abrupt change of MPD were significant predictors for malignant IPMNs ( $p < 0.05$ ). Among texture variables, significant predictors were effective diameter, surface area, sphericity, compactness, entropy, and gray-level co-occurrence matrix entropy ( $p < 0.05$ ). At multivariate analysis, enhancing mural nodule  $\geq 5$  mm (odds ratios (ORs), 6.697 and 6.968, for reviewers 1 and 2, respectively), MPD  $\geq 10$  mm or MPD of 5 to 9 mm (ORs, 4.098 and 4.215, and 2.517 and 3.055, respectively), larger entropy (ORs, 1.485 and 1.515), and smaller compactness (ORs, 0.981 and 0.977) were significant predictors for malignant IPMNs ( $p < 0.05$ ). When adding texture variable to MR findings, diagnostic performance for predicting malignant IPMNs improved from 0.80 and 0.78 to 0.85 and 0.85 in both reviewers ( $p < 0.05$ ), respectively.

**Conclusions** MRCP-derived texture features are useful for predicting malignant IPMNs, and the addition of texture analysis to MR features may improve diagnostic performance for predicting malignant IPMNs.

## Key Points

- Among the MR imaging findings, an enhancing mural nodule size  $\geq 5$  mm and dilated main pancreatic ducts are independent predictors for malignant IPMNs.
- Greater entropy and smaller compactness on MR texture analysis are independent predictors for malignant IPMNs.
- The addition of MR texture analysis improved the diagnostic performance for predicting malignant IPMNs from 0.80 and 0.78 to 0.85 and 0.85, respectively.

**Keywords** Pancreatic neoplasm · Pancreatic cyst · Magnetic resonance imaging · Magnetic resonance cholangiopancreatography · Diagnosis

**Electronic supplementary material** The online version of this article (<https://doi.org/10.1007/s00330-020-07425-0>) contains supplementary material, which is available to authorized users.

✉ Jung Hoon Kim  
jhkim2008@gmail.com

<sup>2</sup> Institute of Radiation Medicine, Medical Research Center, Seoul National University, Seoul, South Korea

<sup>3</sup> Department of Radiology, College of Medicine, Seoul National University, Seoul, South Korea

<sup>1</sup> Department of Radiology, Seoul National University Hospital, 101 Daehak-ro, Jongno-gu, Seoul 03080, South Korea

## Abbreviations

EUS	Endoscopic ultrasound
IPMN	Intraductal papillary mucinous neoplasm
MRCP	Magnetic resonance cholangiopancreatography
ROC	Receiver operating characteristic
SSFSE	Single-shot fast spin echo

## Introduction

With the increasing use and improvement of cross-sectional abdominal imaging, the incidental detection of pancreatic cystic lesions, including intraductal papillary mucinous neoplasms (IPMNs), has increased [1, 2]. The reported prevalence of incidental pancreatic cysts on multidetector computed tomography (CT) or magnetic resonance imaging (MRI) with MR cholangiopancreatography (MRCP) ranges from 2.2 to 19.6% [2]. Since a small percentage of pancreatic cystic lesions progress to invasive cancers and the management strategy can differ based on the malignancy risk, it is important to accurately predict the malignant potential of pancreatic cysts on imaging.

The international consensus guidelines were established in 2006 and recently revised in 2017, suggesting high-risk stigmata and worrisome features on imaging to determine the malignant potential of IPMNs [3]. Moreover, this guideline recommends that only high-risk IPMNs should be resected, while low-risk IPMNs should be managed by surveillance to avoid overtreatment [3]. According to the guideline, endoscopic ultrasound (EUS), CT, and MR imaging with MRCP are recommended as diagnostic and surveillance imaging modalities for pancreatic cysts [3]. Although the usefulness of this guideline has been validated by previous reports [4, 5], the diagnostic performance for predicting the malignant potential of IPMNs by using CT or MR imaging findings before surgical resection is still limited, and the agreement between the preoperative imaging diagnosis and pathologic examination is inadequate in a substantial proportion (30–70%) of cases [6–9].

Recently, texture analysis has received much attention as a quantitative imaging biomarker in oncologic imaging by quantifying tissue heterogeneity and providing important information regarding tumor characterization and prognosis [10, 11]. In a previous study, CT texture analysis of pancreatic IPMNs was shown to be helpful in differentiating malignant IPMNs from benign IPMNs and selecting patients for surgical or nonsurgical management [12, 13]. To the best of our knowledge, however, there have been few studies regarding the usefulness of texture analysis of MR imaging for predicting the malignant potential of pancreatic IPMNs. Thus, the purpose of this study was to investigate the utility of MR findings and texture analysis for predicting the malignant potential of pancreatic IPMNs.

## Materials and methods

### Study population

This retrospective study was approved by our institutional review board, and the requirement of informed consent was waived. Between January 2006 and April 2018, 339 patients with pathologically proven IPMN at surgery were identified through a review of our pathologic database. Among these patients, we included 290 consecutive patients who fulfilled the following inclusion criteria: (1) patients who underwent preoperative pancreas protocol MR examinations including MRCP within 2 months before surgery and (2) patients without any history of local or systemic therapy for pancreatic lesions. We then excluded 41 patients for the following reasons: suboptimal MR image quality with severe motion artifacts or metallic artifacts ( $n = 12$ ), segmentation failure of pancreatic lesions on MRCP source images due to severe motion artifacts ( $n = 27$ ), and segmentation failure due to inability to identify IPMN lesions on MRCP ( $n = 2$ ) (Fig. 1). Therefore, a total of 248 patients (mean age, 69.9 years  $\pm$  10.6 [standard deviation (SD)], 155 men and 93 women) were included in this study. The mean interval between MRI examination and surgery was 15.8 days (range, 1–59 days).

### MR imaging with MR cholangiopancreatography

Pancreatobiliary MR images were obtained using either a 1.5-T ( $n = 58$ ) or 3.0-T ( $n = 190$ ) MR scanner: Signa HDxt 1.5 T (GE Healthcare,  $n = 29$ ); Discovery MR 750w 3.0 T (GE Healthcare,  $n = 3$ ); Magnetom Verio, Magnetom Trio, Biograph mMR, or Skyra 3.0 T (Siemens Healthineers,  $n = 157$ ); and Achieva or Ingenia 3.0 T (Philips Healthcare,  $n = 27$ ) at our institution and various 1.5-T ( $n = 17$ ) or 3.0-T ( $n = 15$ ) scanners at outside

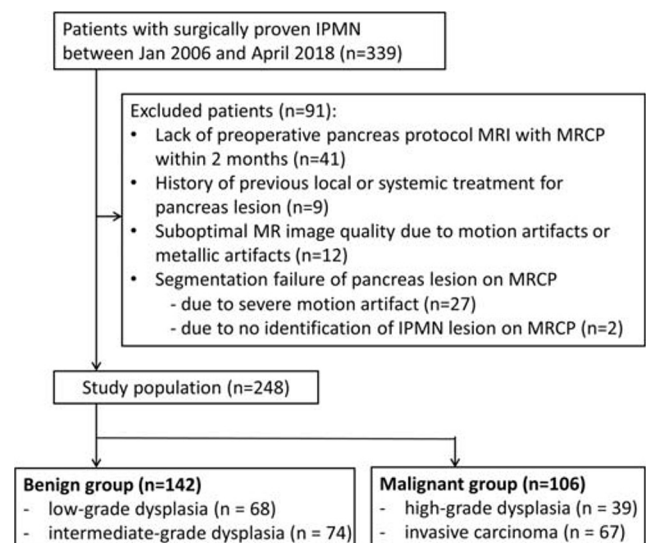


**Fig. 1** Flow diagram of enrolled patients. IPMN, intraductal papillary mucinous neoplasm; MRCP, MR cholangiopancreatography

hospitals. Routine pancreatobiliary MRI included the following sequences: a breath-hold transverse T2-weighted sequence with a single-shot fast spin echo (SSFSE) or a half-Fourier acquisition single-shot turbo spin-echo sequence, a T1-weighted in-phase and opposed-phase spoiled 3D gradient echo sequence, and diffusion-weighted images with  $b$  values of 0 s/mm<sup>2</sup>, 400 s/mm<sup>2</sup>, and 800 s/mm<sup>2</sup>. A dynamic study was performed after the administration of 1.0 mol/L gadobutrol (7.5 mL Gadovist; Bayer Healthcare) at a dose of 0.1 mmol/kg with an injection rate of 2 mL/s. Precontrast imaging was obtained before contrast material injection, and the arterial phase was obtained 8 s after contrast material arrival at the distal thoracic aorta. The portal phase was obtained 60 s after contrast media injection, and the delayed phase was obtained after 2 min, 3 min, and 5 min. MR cholangiography was performed with a coronal respiratory-triggered multisection 3D half-Fourier single-shot turbo spin-echo or single-shot fast spin-echo T2-weighted sequence. After that, 3D MRCP images were reconstructed using a maximum-intensity projection algorithm to produce oblique images rotated about the  $z$ -axis in 10° increments. All parameters for the MR sequences of the two main scanners are summarized in Supplementary Table 1.

### Image analysis

Two abdominal radiologists (S.K.J. and J.Y., with 6 years of experience with abdominal MR imaging each) independently reviewed all MRI examinations using a picture archiving and communication system. Both readers were blinded to the detailed histologic diagnoses but were aware that the study population had pathologically proven IPMN at surgery. Each reviewer recorded whether each IPMN demonstrated any of the high-risk stigmata or worrisome features on MR imaging by referring to the revised 2017 international consensus guidelines (Table 1) [14]. The caliber of the MPD was measured at the maximal point of pancreatic duct dilation. The size of the branch-duct IPMN was measured as the longest diameter in any axial or coronal MRCP image. Enhancing mural nodules were defined as any papillary protruding lesions showing contrast enhancement within the cyst or dilated duct. A thickened and enhancing cyst wall was defined as a cyst wall greater than 2 mm in width with enhancement. All measurements were performed on either axial or coronal images. Lymphadenopathy was defined as enlarged peripancreatic lymph nodes with a maximum short diameter greater than 10 mm. Because this study only evaluated the findings from a single MR examination, the cyst growth rate was not evaluated. In patients with multiple identifiable branch-duct IPMNs, the most suspicious lesion was selected as the target lesion. The most suspicious lesion was defined as the lesion that demonstrated any high-risk stigmata or worrisome features, and if the lesion showed neither high-risk stigmata nor worrisome features, the largest lesion was selected.

**Table 1** Revised 2017 international consensus Fukuoka guidelines for the management of suspected intraductal papillary mucinous neoplasm of the pancreas

Parameter
High-risk stigmata
Obstructive jaundice in a patient with cystic lesion of the head of the pancreas
Enhancing mural nodule $\geq 5$ mm
Main pancreatic duct $\geq 10$ mm
Worrisome features
Pancreatitis (clinical)
Cyst $\geq 3$ cm
Enhancing mural nodule $< 5$ mm
Thickened/enhancing cyst walls
Main duct size of 5–9 mm
Abrupt change in the caliber of pancreatic duct with distal pancreatic atrophy
Lymphadenopathy
Increased serum carbohydrate antigen 19-9
Cyst growth rate $\geq 5$ mm/2 years

### Computerized texture analysis

Lesion segmentation was performed on the source images of MRCP by one radiologist (J.E.K., with 6 years of experience in abdominal imaging) using commercially available software (MEDIP, MEDICAL IP). The software allows semiautomatic identification of lesions with the assistance of the “Hounsfield unit (HU) or signal intensity (SI) threshold” function, which automatically draws all areas within the range of the specific SI defined by the radiologist. After loading the MRCP images into the software, the radiologist drew ROIs using the draw-cut method in a few, selected slice images as follows: (1) within the cyst and (2) outside of the cyst. When drawing (2), the radiologist was assisted by the draw-cut method based on the “SI threshold” function and which automatically drew all areas within the range of the specific SI defined by the radiologist. The software then automatically segmented the cyst. After that, the radiologist modified the extent and margin of the lesion and confirmed its segmentation (Fig. 2). To minimize measurement errors, we used the mean value of the texture parameters obtained from three respective segmentations of the same representative lesion. After segmenting the lesions, the software automatically calculated the texture features, including histogram-based 1st-order statistics, shape- and size-based geometric features, gray-level co-occurrence matrix (GLCM) texture features, and wavelet features [15].

### Pathologic data collection

Information on the type of IPMN, World Health Organization (WHO) grade, and tumor location was collected from the pathologic reports. The type of IPMN was categorized as branch duct, main duct, or mixed type. WHO grade was classified as low-grade dysplasia, intermediate-grade dysplasia, high-grade dysplasia, or associated invasive carcinoma [16].

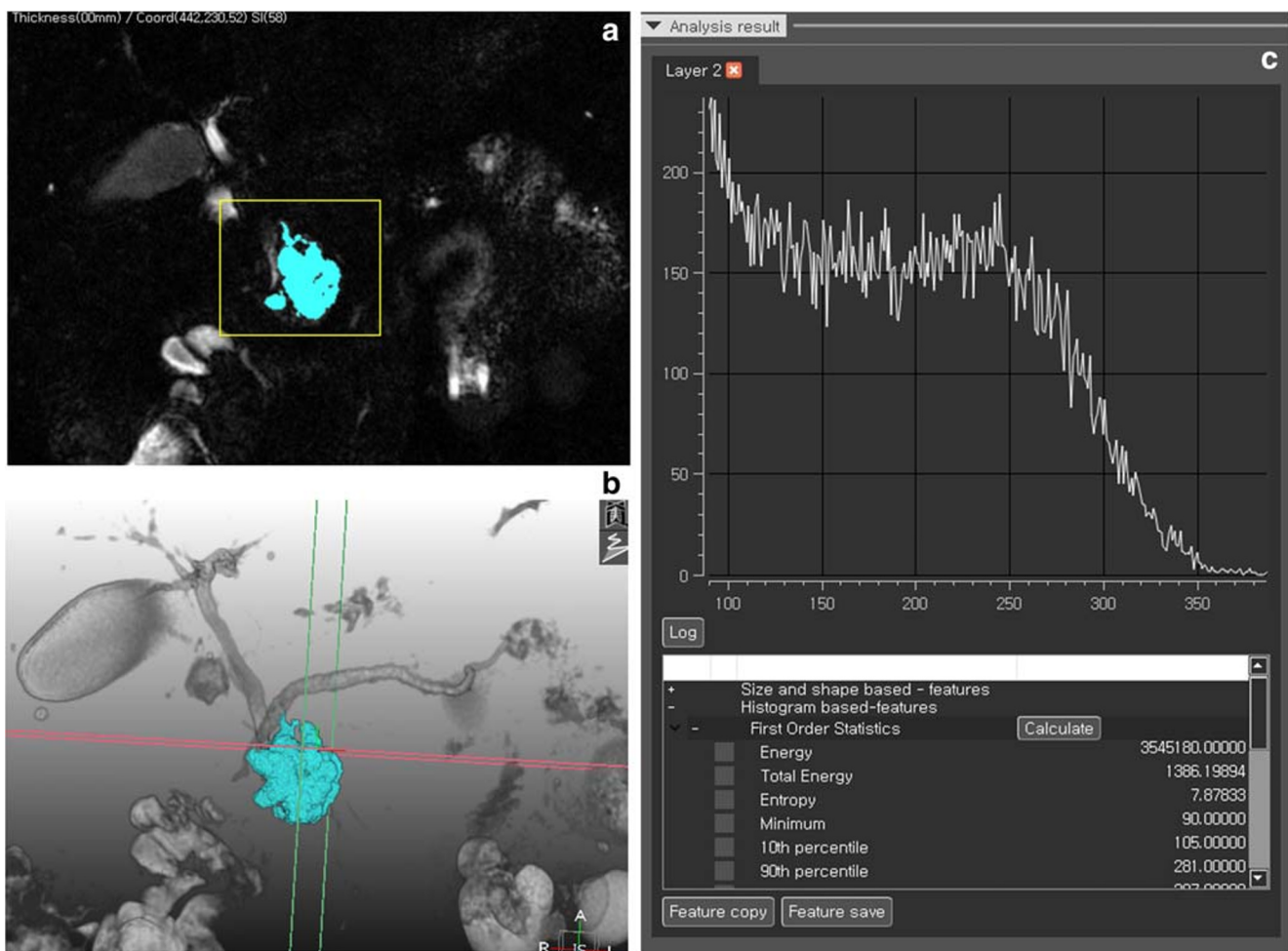


**Fig. 2** MR texture analysis. **a** Semiautomatic lesion segmentation was performed on MR cholangiography (MRCP) source images. After that, the lesion was confirmed on the MRCP source image and maximum

intensity projection (MIP) reconstruction image (**a, b**). **c** Subsequently, texture analysis was performed, and the texture features of the lesions were automatically extracted and calculated

In this study, IPMNs with low- and intermediate-grade dysplasia were classified as benign IPMNs, whereas IPMNs with high-grade dysplasia and associated invasive carcinoma were regarded as malignant IPMNs [5, 17].

### Statistical analysis

The prevalence of clinical or pathologic characteristics and MR findings between malignant IPMNs and benign IPMNs were compared by using the chi-square test or Fisher's exact test for categorical variables and Student's *t* test for continuous variables. Thereafter, logistic regression analyses with the forward projection method were performed to identify significant predictors for malignant IPMN. First, univariable analysis was performed for each image finding and texture parameter, and only variables with *p* values < 0.05 were selected as input variables for multivariable analysis. Receiver operating characteristic analysis was used for regression equations using image findings only as well as for regression equations using image findings and texture variables to evaluate their diagnostic

accuracy for predicting malignant IPMN. To evaluate the interreader reliability of MR findings, the Cohen  $\kappa$  values were calculated and interpreted as follows: 0.81–1.00, excellent agreement; 0.61–0.80, good agreement; 0.21–0.40, fair agreement; and 0.00–0.20, poor agreement. To evaluate the intraexaminer reliability of texture analysis, the intraclass correlation coefficients (ICCs) of three measurement values of each texture variable were calculated and interpreted as follows:  $\geq 0.90$ , excellent;  $\geq 0.75$  to < 0.90, good;  $\geq 0.50$  to < 0.75, moderate; and < 0.50, poor reliability [18]. All statistical analyses were performed by using SPSS software (version 25; IBM), and a *p* value < 0.05 was considered to be statistically significant.

### Results

A total of 142 (57.3%) patients had benign IPMN (68 with low-grade dysplasia and 74 with intermediate-grade dysplasia), and 106 (42.7%) had malignant IPMN (39 with high-



**Table 2** Clinico-pathologic characteristics of the study population

Characteristic	Total (n = 248)	Benign (n = 142)	Malignant (n = 106)	p value
Age (years)*	69.9 ± 10.6	68.3 ± 11.0	71.9 ± 9.8	<i>0.008</i>
Sex				
Male	155 (62.5)	92 (64.8)	63 (59.4)	0.389
Female	93 (37.5)	50 (35.2)	43 (40.6)	
Location				
Head, uncinata	136 (54.8)	78 (54.9)	58 (43.7)	<i>0.010</i>
Body, tail	95 (38.3)	60 (42.3)	35 (33.0)	
Diffuse	17 (6.9)	4 (2.8)	13 (12.3)	
Type of surgery				
Whipple's operation	19 (7.7)	9 (6.3)	10 (9.4)	<i>0.012</i>
PPPD	120 (48.4)	68 (47.9)	52 (49.1)	
Distal pancreatectomy	85 (34.3)	56 (39.4)	29 (27.4)	
Total pancreatectomy	13 (5.2)	2 (1.4)	11 (10.4)	
Central pancreatectomy	11 (4.4)	7 (4.9)	4 (3.8)	
Type of IPMN				
Main duct	33 (13.3)	9 (6.3)	24 (22.6)	<i>&lt; 0.001</i>
Branch duct	113 (45.6)	84 (59.2)	29 (27.4)	
Mixed type	102 (41.1)	49 (34.5)	53 (50.0)	
Pathologic grade of IPMN				
Low-grade dysplasia	68 (27.4)	68 (47.9)		NA
Intermediate-grade dysplasia	74 (29.8)	74 (29.8)		
High-grade dysplasia	39 (15.7)		39 (36.8)	
Invasive carcinoma	67 (27.0)		67 (63.2)	

Unless otherwise specified, data are the number of patients, with percentages in parentheses

PPPD pylorus-preserving pancreaticoduodenectomy, IPMN intraductal papillary mucinous neoplasm

p value < 0.05 indicates a statistical significance and is marked in italics. \*Data are mean ± standard deviation

grade dysplasia and 67 with invasive carcinoma). There were significant differences in age, location of lesion, type of

surgery, and type of IPMN between benign IPMN and malignant IPMN (all *ps* < 0.05) (Table 2).

**Table 3** Comparison of MR imaging findings of benign and malignant IPMNs

Parameter	Reviewer 1			Reviewer 2			Kappa value
	Benign (n = 142)	Malignant (n = 106)	p value	Benign (n = 142)	Malignant (n = 106)	p value	
<b>High-risk stigmata</b>							
Enhancing mural nodule ≥ 5 mm	19 (13.4)	67 (63.2)	<i>&lt; 0.001</i>	25 (17.6)	70 (66.0)	<i>&lt; 0.001</i>	0.731
MPD ≥ 10 mm	15 (10.6)	40 (37.7)	<i>&lt; 0.001</i>	11 (7.7)	34 (32.1)	<i>&lt; 0.001</i>	0.736
<b>Worrisome features</b>							
Cyst size ≥ 3 cm	79 (55.6)	55 (51.9)	0.558	91 (64.1)	57 (53.8)	0.102	0.787
Enhancing mural nodule < 5 mm*	0 (0.0)	1 (0.9)	0.427	0 (0.0)	1 (0.9)	0.427	NA
Thickened/enhancing cyst walls	45 (31.7)	36 (34.0)	0.706	29 (20.4)	21 (19.8)	0.906	0.176
MPD size of 5–9 mm	41 (28.9)	46 (43.4)	<i>0.018</i>	46 (32.4)	51 (48.1)	<i>0.012</i>	0.810
Abrupt MPD change with distal pancreatic atrophy	3 (2.1)	13 (12.3)	<i>0.001</i>	7 (4.9)	26 (24.5)	<i>&lt; 0.001</i>	0.620
Lymphadenopathy*	2 (1.4)	4 (3.8)	0.406	2 (1.4)	4 (3.8)	0.406	0.829

Unless otherwise specified, data are the number of patients, with percentages in parentheses

IPMN intraductal papillary mucinous neoplasm, MPD main pancreatic duct

p value < 0.05 indicates a statistical significance and is marked in italics. \*Fisher's exact test was used

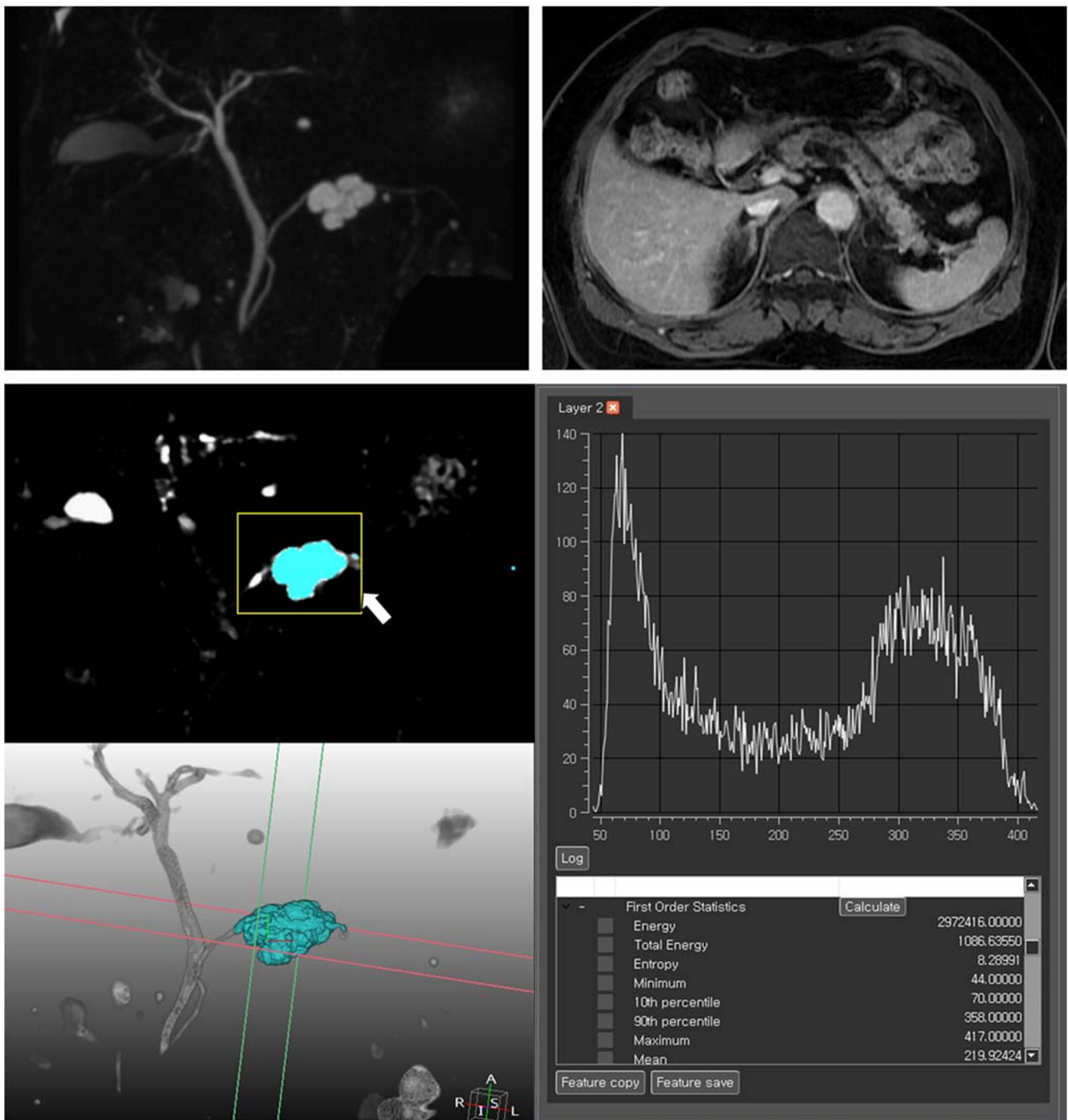


**Fig. 3** Images from a 75-year-old woman who had intraductal papillary mucinous neoplasm (IPMN) with low-grade dysplasia. Maximal intensity projection (MIP) reconstruction image of MR cholangiography (MRCP) shows a 1.8-cm pleomorphic cyst in the

pancreas body without significant pancreatic ductal dilatation. T1-weighted MRI obtained in the portal phase shows no definite enhancing mural nodules or thickened septum. MR texture analysis shows relatively low entropy and high compactness (arrow)

**Comparison of MR imaging features and texture variables between benign and malignant IPMNs**

The MR imaging findings between benign and malignant IPMNs are summarized in Table 3 and Supplementary Table 2. Malignant IPMNs showed significantly higher

frequencies of enhancing mural nodules  $\geq 5$  mm, MPD sizes  $\geq 10$  mm or MPD sizes of 5 to 9 mm, and abrupt MPD changes with distal parenchymal atrophy from both reviewers (1 and 2) (all  $ps < 0.05$ ) (Figs. 3 and 4). In addition, each MRI finding showed good or excellent interobserver agreement ( $\kappa = 0.620\text{--}0.829$ ), except for thickened or enhancing cyst wall,

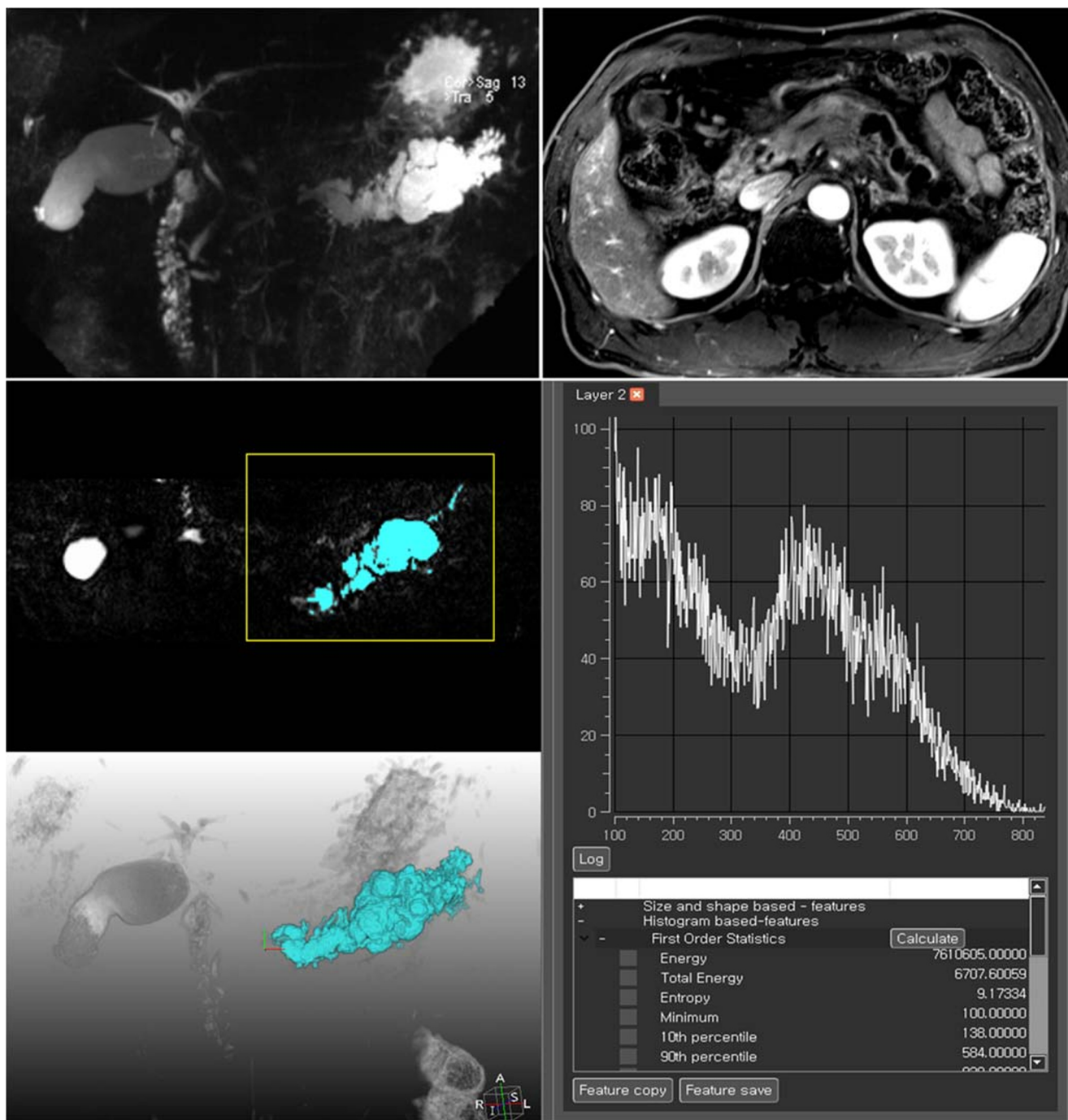


**Fig. 4** Images from a 60-year-old man who had intraductal papillary mucinous neoplasm (IPMN) with invasive carcinoma. MIP reconstruction image of MRCP shows a dilated main pancreatic duct up to 20 mm.

T1-weighted MRI obtained in the portal phase shows an enhancing mural nodule measuring up to 13 mm (arrow). MR texture analysis shows relatively high entropy and low compactness

which showed poor agreement ( $\kappa = 0.176$ ). Table 4, Supplementary Table 3, and Supplementary Table 4 show the comparison of the texture parameters between benign and malignant IPMNs. Several texture variables, including entropy, volume, effective diameter, surface area, sphericity, compactness 2, and GLCM entropy, showed a significant difference between benign and malignant IPMNs ( $ps < 0.05$ ).

### Important MR findings and texture variables for predicting malignant IPMN

In multivariable logistic regression analysis, an enhancing mural nodule size  $\geq 5$  mm (odds ratios (ORs), 6.697 and 6.968; 95% confidence intervals (CIs), 3.431–13.14 and 3.601–13.480;  $ps < 0.001$  for reviewers 1 and 2, respectively),

**Table 4** Comparison of the texture variable of benign and malignant IPMNs

Texture variables	Benign (n = 142)	Malignant (n = 106)	p value
<b>1st-order statistics</b>			
Mean intensity	353.34 ± 24.32	332.65 ± 28.26	0.579
Standard deviation	150.22 ± 10.99	141.97 ± 12.10	0.617
Variance (× 10 <sup>3</sup> )	39.61 ± 6.96	35.53 ± 6.57	0.679
Skewness	0.33 ± 0.06	0.47 ± 0.04	0.084
Kurtosis	-0.26 ± 0.32	-0.49 ± 0.07	0.540
Entropy	8.23 ± 0.08	8.76 ± 0.09	< 0.001
Homogeneity (× 10 <sup>-2</sup> )	2.43 ± 0.23	2.23 ± 0.07	0.446
Uniformity (× 10 <sup>-3</sup> )	4.69 ± 0.74	4.41 ± 0.46	0.764
Energy (× 10 <sup>10</sup> )	1.18 ± 0.39	1.63 ± 0.47	0.463
<b>Geometric features</b>			
Volume (× 10 <sup>3</sup> )	15.51 ± 20.24	31.03 ± 66.20	0.009
Effective diameter	62.81 ± 2.65	81.96 ± 5.49	0.002
Surface area (× 10 <sup>3</sup> )	10.54 ± 1.06	20.97 ± 3.12	0.002
Sphericity	0.53 ± 0.02	0.45 ± 0.02	0.003
Discrete compactness	0.19 ± 0.06	0.02 ± 0.07	0.065
Compactness 1	16.58 ± 0.91	18.40 ± 1.19	0.218
Compactness 2 (× 10 <sup>-3</sup> )	34.64 ± 2.74	17.88 ± 1.53	< 0.001
Roundness (× 10)	7.37 ± 0.03	7.38 ± 0.04	0.877
Moment	2.15 ± 0.41	2.09 ± 0.04	0.295
<b>Texture features (GLCM)</b>			
<b>EW</b>			
GLCM ASM (× 10 <sup>-4</sup> )	2.18 ± 1.10	1.14 ± 0.24	0.418
GLCM IDM (× 10 <sup>-2</sup> )	3.52 ± 0.28	3.52 ± 0.30	0.996
GLCM contrast (× 10 <sup>3</sup> )	7.95 ± 0.83	7.80 ± 1.18	0.735
GLCM entropy	13.84 ± 0.12	14.36 ± 0.14	0.005
<b>NS</b>			
GLCM ASM (× 10 <sup>-4</sup> )	2.20 ± 1.10	1.12 ± 0.22	0.401
GLCM IDM (× 10 <sup>-2</sup> )	3.50 ± 0.29	3.33 ± 0.27	0.657
GLCM contrast (× 10 <sup>3</sup> )	7.36 ± 0.83	7.80 ± 1.18	0.753
GLCM entropy	13.84 ± 0.12	14.36 ± 0.14	0.005
<b>Cross</b>			
GLCM ASM (× 10 <sup>-4</sup> )	1.85 ± 1.10	0.86 ± 0.22	0.440
GLCM IDM (× 10 <sup>-2</sup> )	3.51 ± 0.28	3.42 ± 0.28	0.828
GLCM contrast (× 10 <sup>3</sup> )	7.65 ± 0.82	8.12 ± 1.21	0.743
GLCM entropy	14.49 ± 0.12	14.78 ± 0.15	0.137
<b>SIX</b>			
GLCM ASM (× 10 <sup>-4</sup> )	1.71 ± 1.08	0.76 ± 0.22	0.455
GLCM IDM (× 10 <sup>-2</sup> )	3.39 ± 0.30	3.38 ± 0.31	0.964
GLCM contrast (× 10 <sup>3</sup> )	9.19 ± 1.07	9.05 ± 1.34	0.935
GLCM entropy	14.85 ± 0.13	15.09 ± 0.15	0.230
<b>Wavelet features</b>			
Wavelet_HHH	0.13 ± 0.01	0.15 ± 0.01	0.334
Wavelet_HHL	0.22 ± 0.01	0.22 ± 0.02	0.984
Wavelet_HLH	0.40 ± 0.02	0.41 ± 0.03	0.898
Wavelet_HLL	2.58 ± 0.15	2.46 ± 0.20	0.613
Wavelet_LHH	0.97 ± 0.05	1.04 ± 0.08	0.483
Wavelet_LHL	4.82 ± 0.26	4.63 ± 0.37	0.670
Wavelet_LLH	7.54 ± 0.40	7.39 ± 0.59	0.828
Wavelet_LLL	280.04 ± 22.27	261.31 ± 24.67	0.576

IPMN intraductal papillary mucinous neoplasm, GLCM gray-level co-occurrence matrix. p value <0.05 indicates a statistical significance and is marked in italics

an MPD size ≥ 10 mm (ORs, 4.098 and 4.215; 95% CIs, 1.663–10.097 and 13.619 and 10.973; p = 0.002 and 0.003 for reviewers 1 and 2, respectively), an MPD size of 5 to 9 mm (ORs, 2.517 and 3.055; 95% CIs, 1.209–5.241 and 1.488–6.275; p = 0.014 and 0.002 for reviewers 1 and 2, respectively), greater entropy (ORs, 1.485 and 1.515; 95% CIs, 1.025–2.153 and 1.057–2.171; p = 0.037 and 0.024 for reviewers 1 and 2, respectively), and smaller compactness 2 (ORs, 0.981 and 0.977; 95% CIs, 0.964–0.999 and 0.960–

0.995; p = 0.036 and 0.011 for reviewers 1 and 2, respectively) were found to be independent predictors for malignant IPMNs (Fig. 5). Table 5 and Supplementary Table 5 show the multivariate logistic regression analysis of MR findings and texture analysis variables to predict malignant IPMN.

Using MRI features including the presence of an enhancing mural nodule ≥ 5 mm and an MPD size ≥ 10 mm and an MPD size of 5 to 9 mm, the diagnostic performance for predicting malignant IPMN was 0.80 (95% CI, 0.75–0.85) and 0.79



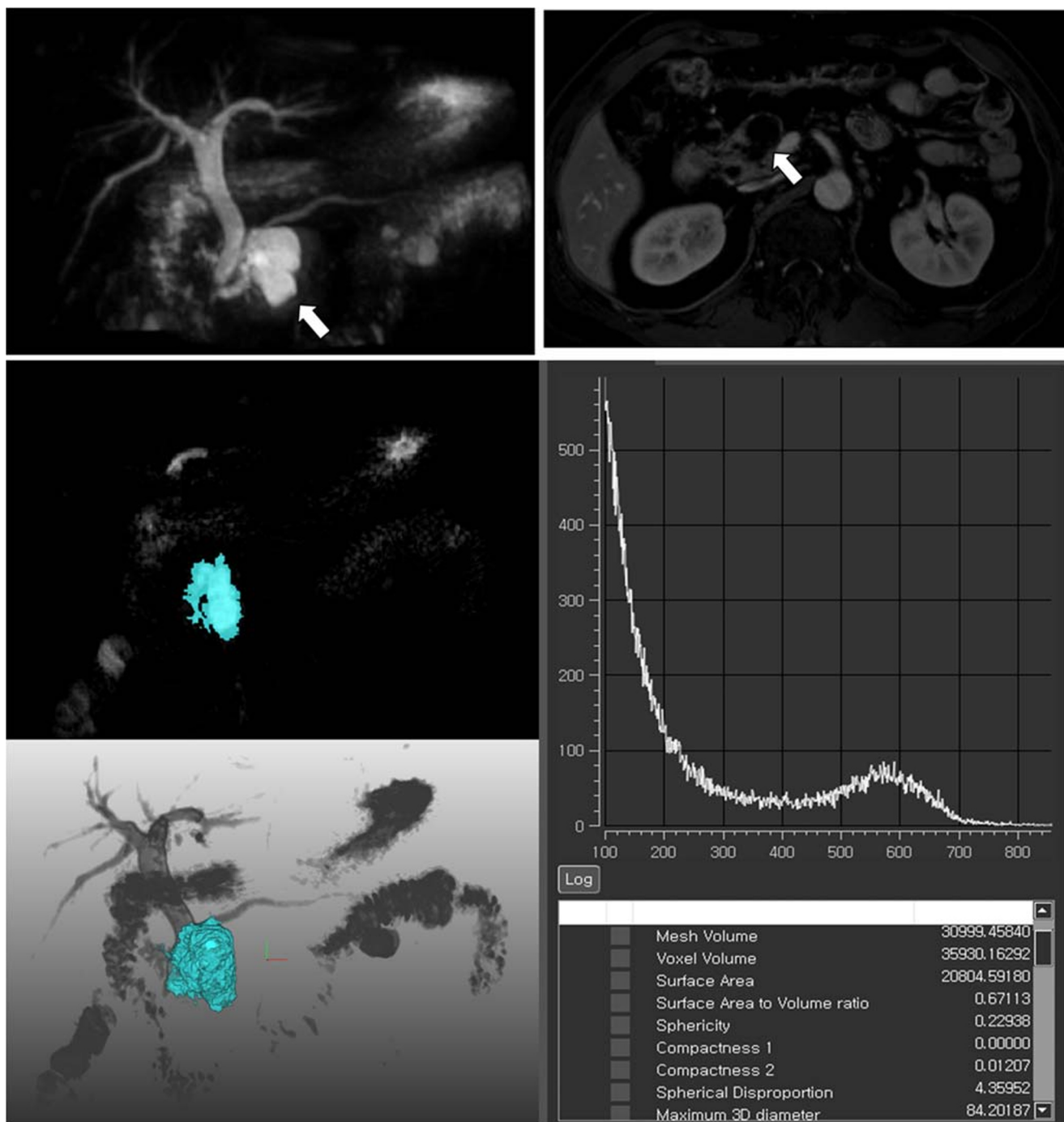


**Fig. 5** Images from a 64-year-old man who had intraductal papillary mucinous neoplasm (IPMN) with invasive carcinoma. MIP reconstruction image of MRCP shows a 3-cm pleomorphic cyst in the pancreas head (arrow) without significant pancreatic ductal dilatation (less than 5 mm).

T1-weighted MRI obtained in the portal phase shows no definite enhancing mural nodules or thickened septum within the cyst (arrow). MR texture analysis shows relatively high entropy and low compactness (arrow)

(95% CI, 0.73–0.84) for reviewers 1 and 2, respectively. When we applied both MR imaging findings and texture variables, including entropy and compactness, the diagnostic performance for predicting malignant IPMN was improved to 0.85 (95% CI, 0.80–0.89) and 0.85 (95% CI, 0.80–0.89) for reviewers 1 and 2 ( $p = 0.021$  and  $0.002$ ), respectively.

## Discussion

Our study demonstrated that an enhancing mural nodule size  $\geq 5$  mm, an MPD size  $\geq 10$  mm or an MPD size of 5–9 mm on MR imaging, greater entropy, and smaller compactness on MR texture analysis were significant predictors for malignant

**Table 5** Multivariate logistic regression analysis of MR findings and texture analysis variables to predict malignant IPMN

Parameter	Reviewer 1		Reviewer 2	
	Odds ratio (95% CI)	<i>p</i> value	Odds ratio (95% CI)	<i>p</i> value
Enhancing mural nodule $\geq 5$ mm	6.697 (3.431, 13.141)	<i>&lt; 0.001</i>	6.968 (3.601, 13.480)	<i>&lt; 0.001</i>
MPD $\geq 10$ mm	4.098 (1.663, 10.097)	<i>0.002</i>	4.215 (1.619, 10.973)	<i>0.003</i>
MPD size of 5–9 mm	2.517 (1.209, 5.241)	<i>0.014</i>	3.055 (1.488, 6.275)	<i>0.002</i>
Entropy	1.485 (1.025, 2.153)	<i>0.037</i>	1.515 (1.057, 2.171)	<i>0.024</i>
Compactness 2	0.981 (0.964, 0.999)	<i>0.036</i>	0.977 (0.960, 0.995)	<i>0.011</i>

IPMN intraductal papillary mucinous neoplasm, MPD main pancreatic duct, CI confidence interval. *p* value  $< 0.05$  indicates a statistical significance and is marked in italics

IPMNs in multivariable analysis ( $p < 0.05$ ). When MR texture variables were added to the MRI findings, the diagnostic performance for diagnosing malignant IPMN improved from AUCs of 0.80 and 0.79 to 0.85 and 0.85 for reviewers 1 and 2, respectively.

Although the imaging features, including the high-risk stigmata and worrisome features suggested by international consensus guidelines, were validated as predictors for malignant IPMNs in many previous studies, the reported diagnostic performance for predicting malignant potential is inadequate (AUCs, 0.637–0.787) [6, 13]. In our study, the diagnostic performance for the prediction of malignant IPMNs was improved up to 0.85 from 0.79 when we applied both MR findings and texture variables. Quantitative image analysis of pancreatic IPMN may have better diagnostic value in predicting malignancy risk than using accepted qualitative radiologic assessment alone, which is also consistent with the results of previous studies using CT texture analysis [12, 13].

Our MR texture analysis results revealed that greater entropy (OR, 1.485–1.515) and smaller compactness (OR, 0.977–0.981) were significant predictors for malignant IPMNs. Entropy is the first-order statistic from the gray-level histogram, reflecting the uniformity of the distribution of the gray level and specifying the randomness in the image values. A greater entropy represents increased tumor heterogeneity, and previous studies have reported that increased tumor entropy suggests tumor aggressiveness and poorer prognosis [10, 12]. Moreover, increased entropy on CT texture analysis [19] and apparent diffusion coefficient histogram metrics [20] were also helpful for predicting malignant IPMNs in previous studies, which is consistent with our study results. Meanwhile, compactness, which is similar to sphericity, is a measure of how compact the shape of the tumor is relative to a sphere, which is considered the most compact. In our study, smaller compactness had a predictive value for malignant IPMNs. Our study results could be explained by the fact that the risk of malignancy in main duct-type IPMNs is higher than that of branch duct-type IPMNs [21], as the value of sphericity and compactness is larger in branch duct-type IPMNs than in main duct-type IPMNs. Therefore, more validation studies will be required for clinical application. In addition, a previous study reported that smaller sphericity or compactness was an important predictor of high-grade (grade 2 or 3) pancreatic

neuroendocrine tumors showing tumor aggressiveness and heterogeneity [22], which is also similar to our result.

Similar to previous reports [6, 23], in our study, an enhancing mural nodule size  $\geq 5$  mm and an MPD size  $\geq 10$  mm, which are high-risk stigmata suggested by the 2017 international consensus guidelines, were independent factors for predicting malignant IPMNs in multivariable analysis. In previous studies, the presence of mural nodules has been one of the strongest predictors of malignant IPMN, and the risk of malignancy increases as the nodule size increases [24]. Our study results also demonstrated that an enhancing mural nodule size  $\geq 5$  mm was the strongest predictor for malignant IPMN, followed by an MPD size  $\geq 10$  mm.

Several limitations of our study need to be mentioned. First, as a retrospective study design, there may be potential selection bias. In addition, as our study population consisted of surgically confirmed IPMNs, it can be a source of selection bias. Because of this specific study population, we think that our study could present the performance of MR findings and texture analysis for predicting malignant IPMNs in patients who consider surgical resection rather than the performance of those findings for the entire population with IPMNs undergoing MRI surveillance. Although our study is meaningful in the prediction of the malignant potential of IPMNs with the pathologic result, which is a concrete reference standard, a large cohort study including all patients with IPMNs undergoing MRI surveillance would be required to validate our study result and reflect clinical practice. Second, the MR scanners used in our study were not uniform across all patients, and interscanner differences may affect the texture analysis results. So, we performed subgroup analysis using a single scanner, and the result of subgroup analysis ( $n = 126$ ) was consistent with the result of total study population ( $n = 248$ ) (Supplementary A, Supplementary Tables 4 and 5). However, further studies with a larger study population and uniform MR scanners and examination protocols are warranted to validate the findings of our study. Third, although tumor segmentation was performed semiautomatically, there may be a potential for measurement error. To minimize the measurement error, repeated measurement was performed in our study, and at intraexaminer reproducibility analysis, texture features showed moderate to high reproducibility (Supplementary Table 3). However, as interexaminer reproducibility was not performed in our study, further study showing interexaminer

reproducibility of texture analysis is warranted. Finally, the texture analysis was only performed by using MRCP images. Due to the high lesion-to-background contrast and thin section thickness of MRCP source images, the volumetric lesion segmentation by using MRCP could be easy and stable. However, other MR images such as DWI or post-contrast images could potentially provide more information regarding malignant potential of IPMNs. Further studies of texture analysis of multiparametric MR images could be helpful. In conclusion, MRCP-derived texture features are useful for predicting the malignant potential of IPMNs, and the addition of texture analysis to MR imaging features may improve the diagnostic performance for predicting malignant IPMNs.

**Funding** The authors state that this work has not received any funding.

### Compliance with ethical standards

**Guarantor** The scientific guarantor of this publication is Joon Koo Han.

**Conflict of interest** The authors of this manuscript declare no relationships with any companies whose products or services may be related to the subject matter of the article.

**Statistics and biometry** No complex statistical methods were necessary for this paper.

**Informed consent** This retrospective study was approved by our institutional review board, and patient informed consent was waived.

**Ethical approval** Institutional review board approval was obtained (IRB No. 1905-018-1031).

### Methodology

- retrospective
- case-control study
- performed at one institution

### References

1. Pandey P, Pandey A, Luo Y et al (2019) Follow-up of incidentally detected pancreatic cystic neoplasms: do baseline MRI and CT features predict cyst growth? *Radiology* 292:647–654
2. Stark A, Donahue TR, Reber HA, Hines OJ (2016) Pancreatic cyst disease: a review. *JAMA* 315:1882–1893
3. Tanaka M, Fernandez-Del Castillo C, Kamisawa T et al (2017) Revisions of international consensus Fukuoka guidelines for the management of IPMN of the pancreas. *Pancreatology* 17:738–753
4. Jang JY, Park T, Lee S et al (2014) Validation of international consensus guidelines for the resection of branch duct-type intraductal papillary mucinous neoplasms. *Br J Surg* 101:686–692
5. Lee JE, Choi SY, Min JH et al (2019) Determining malignant potential of intraductal papillary mucinous neoplasm of the pancreas: CT versus MRI by using revised 2017 international consensus guidelines. *Radiology* 293:134–143
6. Kim KW, Park SH, Pyo J et al (2014) Imaging features to distinguish malignant and benign branch-duct type intraductal papillary mucinous neoplasms of the pancreas: a meta-analysis. *Ann Surg* 259:72–81
7. Roch AM, Ceppa EP, DeWitt JM et al (2014) International consensus guidelines parameters for the prediction of malignancy in intraductal papillary mucinous neoplasm are not properly weighted and are not cumulative. *HPB (Oxford)* 16:929–935
8. Fritz S, Klaus M, Bergmann F et al (2014) Pancreatic main-duct involvement in branch-duct IPMNs: an underestimated risk. *Ann Surg* 260:848–855 discussion 855–846
9. Goh BK, Tan DM, Ho MM, Lim TK, Chung AY, Ooi LL (2014) Utility of the Sendai consensus guidelines for branch-duct intraductal papillary mucinous neoplasms: a systematic review. *J Gastrointest Surg* 18:1350–1357
10. Kim BR, Kim JH, Ahn SJ et al (2019) CT prediction of resectability and prognosis in patients with pancreatic ductal adenocarcinoma after neoadjuvant treatment using image findings and texture analysis. *Eur Radiol* 29:362–372
11. Cassinotto C, Chong J, Zogopoulos G et al (2017) Resectable pancreatic adenocarcinoma: role of CT quantitative imaging biomarkers for predicting pathology and patient outcomes. *Eur J Radiol* 90:152–158
12. Hanania AN, Bantis LE, Feng Z et al (2016) Quantitative imaging to evaluate malignant potential of IPMNs. *Oncotarget* 7:85776–85784
13. Attiyeh MA, Chakraborty J, Gazit L et al (2019) Preoperative risk prediction for intraductal papillary mucinous neoplasms by quantitative CT image analysis. *HPB (Oxford)* 21:212–218
14. Tanaka M, Fernández-del Castillo C, Kamisawa T et al (2017) Revisions of international consensus Fukuoka guidelines for the management of IPMN of the pancreas. *Pancreatology* 17:738–753
15. Aerts HJ, Velazquez ER, Leijenaar RT et al (2014) Decoding tumour phenotype by noninvasive imaging using a quantitative radiomics approach. *Nat Commun* 5:1–9
16. Nagtegaal ID, Odze RD, Klimstra D et al (2020) The 2019 WHO classification of tumours of the digestive system. *Histopathology* 76:182–188
17. Kang HJ, Lee JM, Joo I et al (2016) Assessment of malignant potential in intraductal papillary mucinous neoplasms of the pancreas: comparison between multidetector CT and MR imaging with MR cholangiopancreatography. *Radiology* 279:128–139
18. Koo TK, Li MY (2016) A guideline of selecting and reporting intraclass correlation coefficients for reliability research. *J Chiropr Med* 15:155–163
19. Permuth JB, Choi J, Balarunathan Y et al (2016) Combining radiomic features with a miRNA classifier may improve prediction of malignant pathology for pancreatic intraductal papillary mucinous neoplasms. *Oncotarget* 7:85785–85797
20. Hoffman DH, Ream JM, Hajdu CH, Rosenkrantz AB (2017) Utility of whole-lesion ADC histogram metrics for assessing the malignant potential of pancreatic intraductal papillary mucinous neoplasms (IPMNs). *Abdom Radiol (NY)* 42:1222–1228
21. Salvia R, Crippa S, Partelli S et al (2010) Differences between main-duct and branch-duct intraductal papillary mucinous neoplasms of the pancreas. *World J Gastrointest Surg* 2:342–346
22. Choi TW, Kim JH, Yu MH, Park SJ, Han JK (2018) Pancreatic neuroendocrine tumor: prediction of the tumor grade using CT findings and computerized texture analysis. *Acta Radiol* 59:383–392
23. Shimizu Y, Yamaue H, Maguchi H et al (2013) Predictors of malignancy in intraductal papillary mucinous neoplasm of the pancreas: analysis of 310 pancreatic resection patients at multiple high-volume centers. *Pancreas* 42:883–888
24. Marchegiani G, Andrianello S, Borin A et al (2018) Systematic review, meta-analysis, and a high-volume center experience supporting the new role of mural nodules proposed by the updated 2017 international guidelines on IPMN of the pancreas. *Surgery* 163:1272–1279

**Publisher's note** Springer Nature remains neutral with regard to jurisdictional claims in published maps and institutional affiliations.